MDPI

*Article*

# Application of Electric Field Force for the Accumulation of Anthocyanins from Winery Wastewater

Vasileios Bartzis [1,*], Irini F. Strati [1] , Ioannis E. Sarris [2,*] , Thalia Tsiaka [1], Anthimia Batrinou [1] , Spyros J. Konteles [1] and Vassilia J. Sinanoglou [1]

[1]   Department of Food Science and Technology, Faculty of Food Science, University of West Attica, Campus Alsos Egaleo, Ag. Spyridonos 28, Egaleo, 12243 Athens, Greece; estrati@uniwa.gr (I.F.S.); tsiakath@uniwa.gr (T.T.); batrinou@uniwa.gr (A.B.); skonteles@uniwa.gr (S.J.K.); vsina@uniwa.gr (V.J.S.)

[2]   Department of Mechanical Engineering, University of West Attica, 12244 Athens, Greece

[*]   Correspondence: vbartzis@uniwa.gr (V.B.); sarris@uniwa.gr (I.E.S.)

**Abstract:** The recovery of anthocyanins from winery wastewater constitutes an attractive option for both environmental and commercial valorization, as food colorants and nutraceutical ingredients. In this study, the electric field induced ion drift method is proposed as a promising technique for the purification of wastewater solutions as well as for the accumulation of anthocyanins. The cation of the anthocyanidin malvidin ($C_{17}H_{15}O_7^+$) was selected as the most representative of winery waste, in order to develop a theoretical model. The main principle of the model is based on the displacement of charged anthocyanin ions, under the influence of an electric field vertical to the flow of the solution, and their accumulation on the side walls of a conductor. Apparatus inducing an electric field drift is described, and critical parameters (i.e., final spatial distribution of concentration, electric field intensity, surface charge density, and potential) were calculated. The proposed model succeeded in reducing anthocyanin concentration by more than 90%, for duct widths smaller than 1 mm in the bulk of the solution, for applied potentials $\varphi(0)$ in the range of 0.2–0.4 V and target concentrations equal to $1.2 \times 10^{-3}$ mol/m$^3$.
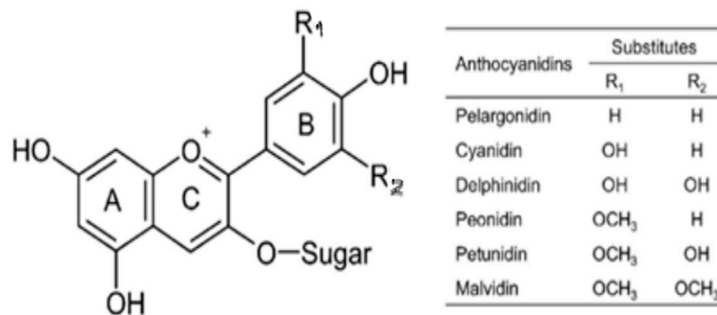
## 1. Introduction

Wine production is a large industry worldwide, generating significant amounts of waste. The effluent from wine factories has a low pH and high organic pollutants because it contains carbohydrates, lipids, proteins, and phenolic compounds [1]. Additionally, the inorganic compounds of winery wastewater are largely dependent upon the nature of the cleaning agents used in wineries and upon the potassium ions naturally present in grapes [2].

Effluent disposal can lead to negative environmental effects: more specifically, to the death of aquatic organisms and to the generation of foul odors resulting from the decrease in oxygen levels in aquatic media due to high Chemical Oxygen Demand (COD) values [3]. In addition to the high organic/inorganic load of the winery effluent, its treatment presents certain difficulties mostly related to the management of large volumes of water with significant seasonal variation. These processes include physicochemical, biological, membrane filtration, and separation processes, as well as treatments combining biological and advanced oxidation processes [4].

Winery wastewater represents a potential source of bioactive constituents, with flavonoids being the most important. Among the flavonoids, anthocyanins, proanthocyanidins (procyanidins and prodelphinidins), and flavan-3-ols are present in significant amounts. More specifically, total anthocyanin content ranges from 131.00 to 1790.00 mg/100 g of dry matter of winery effluent [5].

Anthocyanins are pigments responsible for the color variability of many fruits, flowers, and vegetables. They are claimed to have many health benefits, including anti-inflammatory, anti-cancer, and antioxidant properties [6]. Regarding their chemical structure, anthocyanins are considered as glycosides of the following six anthocyanidins: pelargonidin (Pg), cyanidin (Cy), peonidin (Pn), delphinidin (Df), petunidin (Pt), and malvidin (Md), which differ in number and position of $CH_3O-$ and $OH-$ groups in ring B (Figure 1). On the other hand, anthocyanins mainly present integrated di-, tri-, or mono-saccharide units into an anthocyanidin structure. The most common carbohydrate residue molecules are glucose, rhamnose, galactose, and arabinose [7].



| Anthocyanidins | Substitutes | |
|---|---|---|
| | $R_1$ | $R_2$ |
| Pelargonidin | H | H |
| Cyanidin | OH | H |
| Delphinidin | OH | OH |
| Peonidin | $OCH_3$ | H |
| Petunidin | $OCH_3$ | OH |
| Malvidin | $OCH_3$ | $OCH_3$ |

**Figure 1.** Chemical structure of the flavylium cation (**left**). The specific substitutes at $R_1$ and $R_2$ positions forming the main anthocyanidins are listed on the (**right**) side.

Anthocyanin pigments are mainly influenced by many factors such as temperature, pH, light, oxygen, metallic ions, and certain solvents. The 3-O-glycosides of malvidin, petunidin, cyanidin, peonidin, and delphinidin are the principal anthocyanins found in grape skins [7].

The recovery of anthocyanins from winery wastewater constitutes an attractive option for both environmental and commercial valorization, as food colorants and nutraceutical ingredients. The prevailing extraction techniques for the recovery of anthocyanins comprise the application of organic solvents, subcritical water, supercritical carbon dioxide ($CO_2$), pressurized liquid, and microwave and ultrasound extractions. Lately, the application of ionic liquids, deep eutectic solvents, as well as compressed and supercritical fluids has been suggested as an "eco-friendly" alternative to traditional organic solvents for the extraction of these pigments [8].

Nevertheless, most of these methods require extensive processing, resulting in high costs and potential losses in terms of extract quality and quantity. Therefore, there is a need for new, efficient, and cost-effective techniques for the recovery of anthocyanins from winery wastewater. High Voltage Electrical Discharge (HVED) and Pulsed Electric field (PEF) are non-thermal, electric treatment processes based on different extraction principles, which maintain the quality of the extracted compounds. HVED is a technique that allows achieving fair performance using low-energy input and low organic solvent volumes. On the other hand, PEF technology is also considered to be a low-energy process, which relies on cell permeability and promotes mass transfer by the diffusion of metabolites. A short pulsed electric field causes a temporary destabilization of the cell membrane due to its charging and polarization [9].

The electric field induced ion drift method has been successfully implemented for water desalination as well as for water purification from heavy metals and bacterial toxins [10–14]. A similar analysis conducted on nanochannels [15–17] using molecular resolution simulation found that this method can efficiently remove ions. Recently, computational investigations on the effects induced by external electric fields on liquid water [18] and, more generally, on liquid systems [19] were developed. An electric field is created by a capacitor, which is placed outside a conductor. An aqueous solution containing ions flows into the conductor and, under the influence of the electric field, the electrically charged molecules are forced to migrate towards a specific pole of the capacitor. Therefore, a decrease in ion concentration

is observed in most of the solution, while their concentration increases at the side walls of the conductor.

The application of an electric field induces various phenomena, such as electrophoresis, electro-osmosis, and dielectrophoresis [20], which can enhance the separation and recovery of anthocyanins from the complex matrix of winery wastewater. Electric field induced drift of anthocyanins from winery wastewater is a promising technique for the recovery of these valuable compounds. Additionally, electric field induced drift can be an eco-friendly and cost-effective technique, requiring little or no chemical reagents, and can be easily scaled up for industrial applications.

In the present study, an attempt was made for the development of a theoretical model based on the electric field induced ion drift method, in order to recover anthocyanins from winery wastewater. For this reason and in order to build the model, preliminary physicochemical treatment, namely ion exchange or reverse osmosis, was required in order to effectively remove small cations, such as $Na^+$, $K^+$, $Ca^{++}$, and $Mg^{++}$ [2]. The cation of anthocyanidin malvidin ($C_{17}H_{15}O_7^+$) was selected as the most representative of winery waste. The apparatus used to induce an electric field drift is described and the critical parameters involved, i.e., the final spatial distribution of the concentration, the electric field strength, the surface charge density, as well as the potential, were calculated. In a further step, the integration time required for displacement was estimated using the Nernst Planck equations in the linear regime for low voltages, as a function of the channel width and final concentration.

## 2. Description of the Theoretical Model

### 2.1. Characteristics of Anthocyanidin

Table 1 presents the basic characteristics of anthocyanidin.

**Table 1.** Characteristics of anthocyanidin, $C_{17}H_{15}O_7^+$.

| Molecular Weight (MW) | 331.30 | Helmholtz Capacitor Effective Width $\lambda_S$ (nm) | 0.46 | $\varphi_s^{max}$ (V) | 0.3724 |
|---|---|---|---|---|---|
| Volume (nm$^3$/particle) | 0.402 | Effective radius r (nm) | 0.46 | $\varphi_{max}(0)$ (V) | 0.4292 |
| Net charge (at pH 7.4) z | 1 | Mass (g/particle) | $5.501 \times 10^{-22}$ | $C_M$ (mol/m$^3$) | 0.0012 |
| Density (g/cm$^3$) | 1.37 | Debye screening length $\lambda_D$ (m) | $2.8 \times 10^{-7}$ | | |
| $C_{max}$ (mol/m$^3$) | 2167.32 | Diffusion coefficient D (m$^2$/s) | $3.5 \times 10^{-10}$ | | |

Notes: $\varphi_{max}(0)$: maximum potential at y = 0. $\varphi_s^{max}$: Outer Helmhotz Plane (OHP) maximum potential at y = 0. $C_M$: final anthocyanin concentration (after electric field application) in the center of the duct.

### 2.2. Experimental Layout of the Anthocyanidin Ion Drift Model

The principal hypothesis made for the theoretical model is that winery wastewater containing anthocyanins should have been adequately pretreated for the reduction of its organic load and for the retention of charged anthocyanidins. Figure 2 presents the experimental layout of the ion drift model. As the solution flows into the duct of the device, the application of an electric field forces the charged ions to move to the side walls of the duct, attracted by the positive and negative electrodes, accordingly.

The device consists of the following individual components:

- A capacitor with two electrodes, to which voltage V is applied; therefore, a homogeneous electric field is created in the y direction to the negative electrode. The charged capacitor together with the duct into which the solution flows is presented in Figure 3, which also shows the accumulation of ions on both sides of the duct depending on their charge
- A main duct of insulating material into which the solution to be treated flows along the electrodes.
- Two smaller ducts inside the main duct close to the side walls, for collecting part of the solution with increased ion concentration.
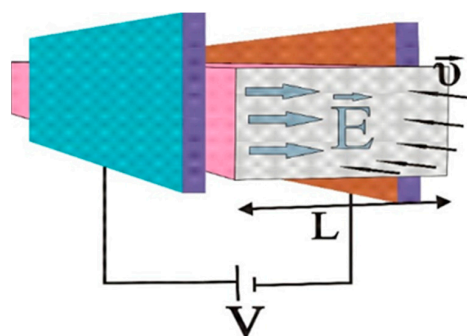
**Figure 2.** Experimental layout of the anthocyanidin drift model (V: capacitor voltage; L: width of the duct; E: electric field intensity; $\vec{v}$: velocity of solution).
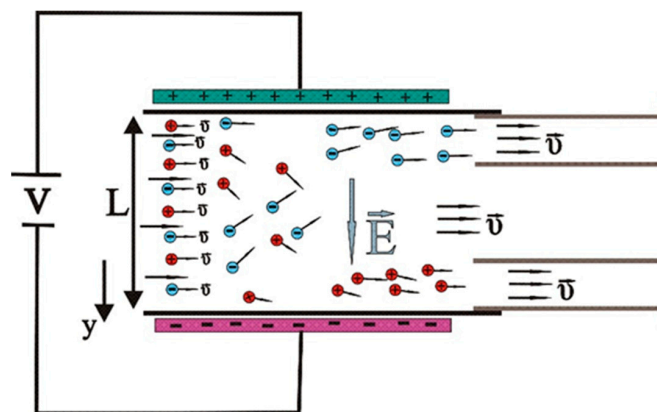


**Figure 3.** Anthocyanidin ion movement inside the duct (V: capacitor voltage; L: duct width; E: electric field intensity along y axis; $\vec{v}$: velocity of solution).

The gap between the electrodes and the duct should be kept to a minimum to ensure homogeneity in space of the external electric field. In this way the solution flows vertical to the electric field with speed $\vec{v}$. In a first approximation, we consider that the speed across the width of the duct remains spatially constant. Due to the lateral accumulation of ions, there is a change in their concentration along the y axis, as presented in Figure 4.
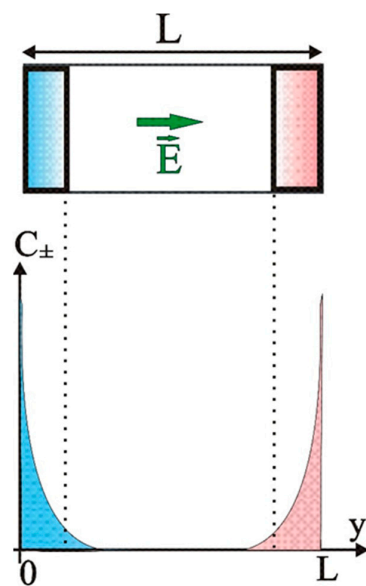


**Figure 4.** Schematic presentation of ion concentration across the duct (L: duct width; $C_{\pm}$: concentation of the positive (red color) and negative (blue color) ions).

### 3. Creation of Stern Model Double Layer

*3.1. Description of the Theoretical Model*

The large size of the studied molecules, along with the fact that they are neither compact nor defined in shape, sets certain limitations. Two assumptions were made: the first one is that ions are globular with an effective radius of 0.46 nm (Table 1), and the second one is that during their movement the ions do not deform or decay. Taking into consideration the dimension of the ions, their radius being the shortest distance from the walls of the duct, this describes the Stern model. According to this model, a double layer is formed near each electrode, consisting of two individual parts [21,22]:

(a)  A compact layer, which is also known as the Stern layer, is formed by ions in contact with the walls of the duct. It can be equated to a capacitor (Helmholtz capacitor) with capacity per unit area $c_H$:

$$c_H = \frac{\varepsilon}{\lambda_S} \tag{1}$$

where its effective width $\lambda_S$ is considered equal to the ion radius (Table 1). Throughout the subsequent analysis, the electric permittivity of water is $\varepsilon = \varepsilon_r \varepsilon_0$, which is considered a continuous medium [23–25] with $\varepsilon_r \approx 80$ its relative permittivity and $\varepsilon_0 = 8.85 \times 10^{-12}$ F/m the vacuum permittivity.

(b)  A diffuse layer is created beyond the compact layer and is comparable to a capacitor with capacity per unit area $c_D$:

$$c_D = \frac{\varepsilon}{\lambda} \tag{2}$$

where $\lambda$ is its effective width according to the Gouy–Chapman theory (Figure 5).
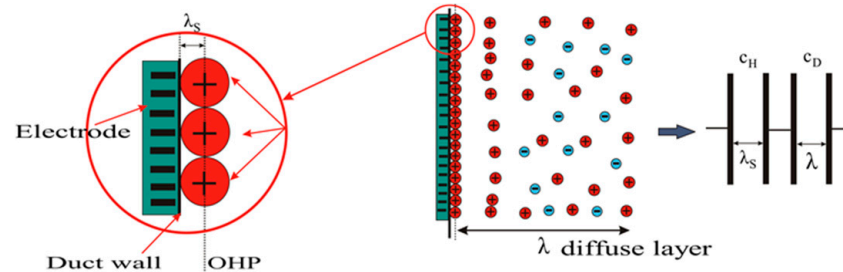


**Figure 5.** Representation of the double layer; OHP: Outer Helmholtz Plane. Positive ions are in red and negative in blue.

The boundary conditions should be determined. We consider that the two sides of the duct, which are in positions y = 0 and y = L, have potentials $\varphi(0)$ and $-\varphi(0)$, respectively. Thus, in the center of the duct the potential is considered zero $\varphi(y = \frac{L}{2}) = 0$. Considering that the potential varies linearly with the distance within the compact layer, we have:

$$\varphi = \pm \varphi(0) \pm \lambda_s \frac{\partial \varphi}{\partial y} \text{ for } y = 0, L \tag{3}$$

The total electric field across the duct is created by two sub-electric fields. The first one is the external electric field that is created between the electrodes and is almost homogeneous, as already mentioned. The second electric field, which is due to the accumulation of charges on both sides of the duct, is opposite to the first one and increases with time as accumulation of the load grows.

### 3.2. Final State Parameters

Surface charge density ($\sigma$) (the amount of charge per unit area) near the positive and negative electrodes is calculated [8] as follows:

$$\sigma = -\sqrt{8\varepsilon C_M RT}\,\sinh\!\left[\frac{zF}{2RT}\left(\frac{\sigma\lambda_s}{\varepsilon} + \varphi(0)\right)\right] \tag{4}$$

where $C_M$ is the final (after electric field application) anthocyanin concentration in the center of the duct, $T = 300$ K is the absolute temperature which is considered constant, z is the number of excess positive or negative charges (considered positive), $R = 8.314$ J/(mol·K), and $F = 96{,}485.34$ C/mol is the Faraday constant.

$C_M$ is considered critical to our study. Practically, $C_M$ will remain constant for most of the duct width, except for its edges, in which we will have a large ion concentration.

In the following analysis we consider a target value $C_M$, expressed in mol/m³ as:

$$C_M = 1.2 \cdot 10^{-3}\ \text{mol/m}^3 \tag{5}$$

Figure 6 presents surface change density $\sigma$ as a function of $C_M$, for different $\varphi(0)$ values. It can be noticed that the surface charge density increases with increasing $C_M$; however, there is a larger increase in surface charge density with increasing $\varphi(0)$.
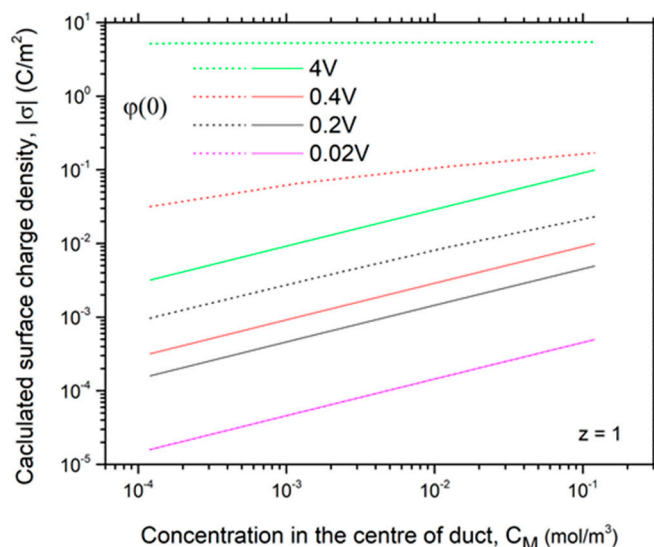


**Figure 6.** Calculated surface charge density $|\sigma|$ (C/m²) as a function of $C_M$ (mol/m³) of anthocyanins for different electric potential values $\varphi(0)$ (V) (dotted lines). Solid lines represent the corresponding $|\sigma_l|$ values in the linear regime.

The constant electric field intensity inside the compact layer is calculated in Equation (6):

$$E_{\lambda_S} = \sqrt{\frac{8 C_M RT}{\varepsilon}}\,\sinh\!\left[\frac{zF}{2RT}\left(-\lambda_s E_{\lambda_S} + \varphi(0)\right)\right] \tag{6}$$

while, outside of the compact layer, the electric field intensity is given by Equation (7):

$$E = -\frac{\partial \varphi}{\partial y} = \sqrt{\frac{8 C_M RT}{\varepsilon}}\,\sinh\!\left(\frac{zF}{2RT}\varphi\right) \tag{7}$$

where

$$\varphi = \frac{4RT}{zF}\tanh^{-1}\!\left\{\tanh\!\left(\frac{zF\varphi_s}{4RT}\right)\cdot e^{-\kappa(y-\lambda_s)}\right\}\ \text{for}\ \lambda_s \le y \le {}^{L}\!/_{2} \tag{8}$$

and

$$\varphi = \frac{4RT}{zF}\tanh^{-1}\left\{-\tanh(\frac{zF\varphi_s}{4RT})\cdot e^{\kappa(y-L+\lambda_s)}\right\} \text{ for } {}^L/_2 \le y \le L-\lambda_s \tag{9}$$

where $\lambda_s = 0.46$ nm (Table 1), $\kappa = \left[\sqrt{\frac{\varepsilon RT}{2z^2C_MF^2}}\right]^{-1}$, and $\varphi_s$ is the Outer Helmholtz Plane (OHP) given by Equation (10):

$$\varphi_S = \varphi(0) - \lambda_s\sqrt{\frac{8C_MRT}{\varepsilon}}\sinh(\frac{zF}{2RT}\varphi_s) \tag{10}$$

In the case of anthocyanins, both areas are of interest to us: the one that will remain free from them, but also the area in which anthocyanins will accumulate and which is located on the sides of the duct. To calculate the area in which the excess anthocyanins accumulate, the total differential capacitance needed is $c_{tot}$, defined as:

$$c_{tot} = \frac{|d\sigma|}{d\varphi(0)}$$

Total differential capacitance $C_{tot}$ is calculated using Equation (4), as follows:

$$c_{tot} = \frac{\sqrt{\frac{2C_M\varepsilon z^2F^2}{RT}}\cosh(\frac{zF}{2RT}\varphi_s)}{1+\frac{\lambda_s}{\varepsilon}\sqrt{\frac{2C_M\varepsilon z^2F^2}{RT}}\cosh(\frac{zF}{2RT}\varphi_s)} \tag{11}$$

As already mentioned, according to the Stern model, the double layer consists of the compact layer (Stern layer) with capacity $c_H$ in series with the diffuse layer with differential capacity $c_D$, as follows (Figure 4):

$$c_H = \frac{\varepsilon}{\lambda_s}$$

$$c_D = \sqrt{\frac{2C_M\varepsilon z^2F^2}{RT}}\cosh(\frac{zF}{2RT}\varphi_s)$$

In addition, $c_D$ can be alternatively written as:

$$c_D = \frac{\varepsilon}{\lambda_D}\cosh(\frac{zF}{2RT}\varphi_s) \tag{12}$$

where

$$\lambda_D = \kappa^{-1} = \sqrt{\frac{\varepsilon RT}{2z^2C_MF^2}} \tag{13}$$

is the Debye screening length (the width of the diffuse layer in the linear regime) ($\lambda_D$ value in Table 1).

If $c_D$ is expressed as $c_D = \frac{\varepsilon}{\lambda}$, we have:

$$\frac{\lambda}{\lambda_D} = \left[\cosh(\frac{zF}{2RT}\varphi_s)\right]^{-1} \tag{14}$$

where $\lambda$ is the length of the diffuse layer, i.e., the effective width in which the anthocyanins are crammed.

Figure 7 presents $\frac{\lambda}{\lambda_D}$ as a function of $\varphi(0)$ (Equation (14) in combination with Equation (10)) for different values of $C_M$.
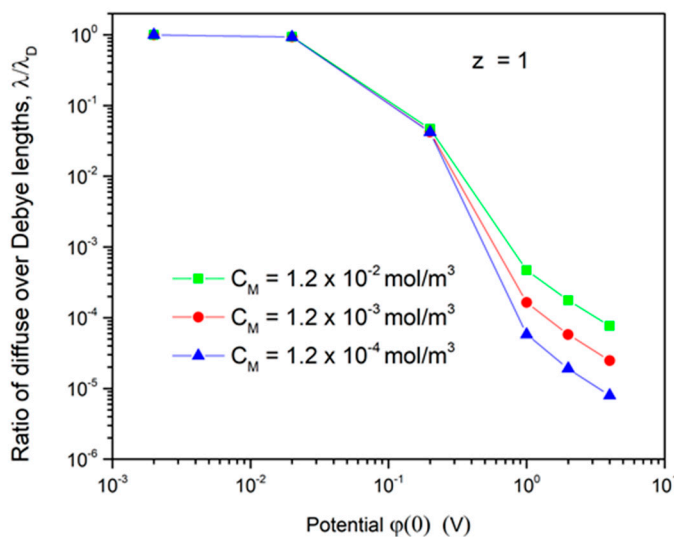
**Figure 7.** Ratio of $\lambda/\lambda_D$ for anthocyanins as a function of $\varphi(0)$ (V) for different $C_M$ values.

The physical meaning of $\lambda$ is that it denotes the effective width of the area into which the anthocyanin ion charges are crammed when the electric field is applied. It is therefore legitimate for this width to be as small as possible. From Figure 7, it is evident that $\lambda$ decreases with an increase in potential. For potentials of the order of 0.2–0.3 V, $\frac{\lambda}{\lambda_D}$ is of the order of $10^{-2}$. This means that $\lambda$ is of the order of $\sim 10^{-9}$ m, which is negligible in relation to the width of conductor L, which is at least $L \sim 10^{-4}$ m. Conclusively, most of the duct remains free of anthocyanins, which are accumulated on its side walls. Using ducts of small internal diameter, both drained water as well as a solution with a high concentration of anthocyanins can be collected, as presented in Figure 3.

Throughout the above analysis, it was assumed that the ions follow Boltzmann distribution. This is true outside the compact layer. For negatively charged ions, attracted to the positive electrode, the concentration is given by Equation (15):

$$C_- = C_M e^{+\frac{zF}{RT}\varphi} \tag{15}$$

where potential $\varphi$ is given by Equations (8) and (9). Equation (15) can also be used for positively charged ions, because the distribution of anthocyanin concentration is symmetrical. In addition, $C_M$ is anthocyanin concentration in the center of the duct, after the influence of the electric field, and is equal to:

$$C_M = 1.2 \cdot 10^{-3} \text{ mol/m}^3$$

If $C_0$ is the uniform density of the anthocyanins in the initial solution (before the application of the electric field), its relation to $C_M$ is given by:
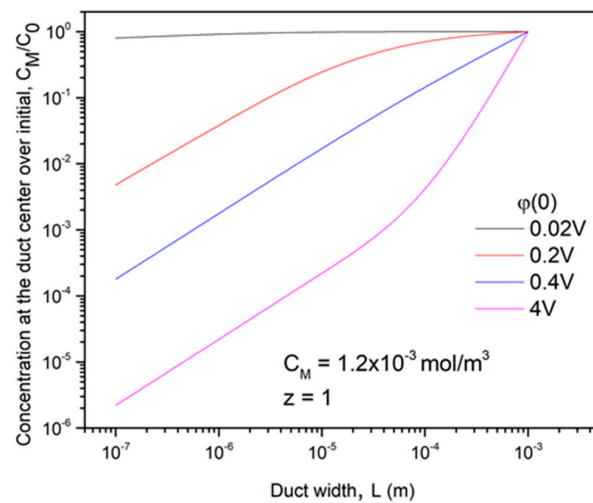
$$C_0 = \frac{C_M \int_{\lambda_s}^{L-\lambda_s} e^{+\frac{zF}{RT}\varphi} dy}{L}$$

or

$$\frac{C_M}{C_0} = \frac{L}{\int_{\lambda_s}^{L-\lambda_s} e^{+\frac{zF}{RT}\varphi} dy} \tag{16}$$

In Figure 8, fraction $\frac{C_M}{C_0}$ is represented as the function of duct width L, for different potential values, with the desired final concentration, $C_M = 1.2 \cdot 10^{-3} \text{ mol/m}^3$.

**Figure 8.** $C_M/C_0$ for anthocyanins as a function of duct width L (m) and target concentration $C_M = 1.2 \times 10^{-3}$ mol/m$^3$ for different potential $\varphi(0)$ (V) values.

As previously discussed, the numerator of the fraction refers to the concentration of anthocyanins in the main volume of the solution after applying an electric field, which remains constant. Conversely, the denominator represents the uniform concentration of anthocyanins before applying the field. A larger denominator leads to a smaller fraction. Consequently, a smaller fraction indicates more favorable outcomes. Figure 8 clearly illustrates that increasing the potential and reducing the width of the duct both diminish ratio $C_M/C_0$. An initial observation reveals that when the value of $\varphi(0)$(V) is lower (corresponding to the linear approximation), there is no significant decrease in concentration (represented by the black line). However, when the potentials are ten or twenty times higher than the minimum value and the duct width is less than 1 mm, the decrease in concentration in the main volume of the solution becomes substantial, reaching 90% (as shown by the red and blue lines in Figure 8). With further increases in potential, the anthocyanin concentration in the main volume of the solution almost entirely diminishes (represented by the pink line). It should be noted, however, that these effects (occurring for values greater than 0.4 V; pink line in Figure 8) have qualitative importance only, as steric effects become significant, as will be discussed in the following paragraph.

*3.3. Model Validity*

Detailed discussion on the limitations and considerations of the aforementioned theoretical analysis will be presented. Firstly, it is important to note that in the final equilibrium state, the concentration of charged anthocyanins follows the Boltzmann distribution

$$C_- = C_M e^{+\frac{zF}{RT}\varphi} \tag{17}$$

This has a condition that the electrochemical potential is of the form:

$$\widetilde{\mu} = \mu_0 + RT\ln C_- + ze\varphi \tag{18}$$

The validity of Equation (18) relies on the assumption that the solution is dilute and the ions are treated as ideal particles with negligible size. Despite the ions themselves being relatively large in size, Equation (18) remains applicable as long as the concentration is low, as this is necessary for the ions to be adequately separated from each other. The size of the ions imposes a constraint on the maximum attainable concentration at the transition point from the compact layer to the diffuse layer [26–28]. The imposed limit cannot exceed the following value:

$$C_{max} = \frac{1}{N_A a^3} \tag{19}$$

where $a = 2r$ is the effective diameter of an anthocyanidin ion (Table 1). From the relationship relating $C_{max}$ with $\varphi_s^{max}$:

$$C_{max} = C_M e^{+\frac{zF}{RT}\varphi_s^{max}}$$

we have

$$\varphi_s^{max} = \frac{RT}{zF}\ln\left(\frac{C_{max}}{C_M}\right) \tag{20}$$

The value of $\varphi_{max}(0)$ representing the maximum potential for which the aforementioned model remains valid is calculated using Equation (10) ($\varphi_{max}(0) \sim 0.4$ V) (as shown in Table 1). However, it should be noted that these values should be considered indicative rather than definitive. The closer we approach these values, the less applicable the dilute solution approximation becomes, which is necessary for Boltzmann distribution.

## 4. Estimation of Time in the Linear Approximation

An essential parameter to consider is the time required for the phenomenon to complete. This estimation can only be achieved by employing the Poisson Nernst Planck (PNP) equations in a linear regime. The linear approach can be applied only when the applied potential is small, i.e.,

$$\left| z\frac{F}{RT}\varphi(0) \right| < 1 \text{ or } z \cdot \varphi_l^{max}(0) = 0.026 \text{ V} \tag{21}$$

where $\varphi_l^{max}$ is the maximum potential for which the linear approximation is applied. The surface charge density in the linear regime ($|\sigma_l|$) [8] is given by the relationship:

$$|\sigma_l| = \varphi(0)\frac{\varepsilon}{(\lambda_S + \kappa^{-1})} \tag{22}$$

The surface charge density in the linear regime ($|\sigma_l|$) can be expressed as a function of $C_M$, using Equation (22). This relationship is crucial for ensuring the validity of the preceding analysis. In Figure 6, the solid lines depict the surface charge density in the linear model, while the dotted lines represent the exact calculation using the Stern model. Notably, for small potentials, the linear model (pink line) and the Stern model calculation (pink dotted line) coincide. However, as the potentials increase, they start to diverge. This observation confirms the validity of both analyses: the linear model is appropriate for small potentials, while Stern model analysis is suitable for higher potentials.

Regarding the estimation of time, a time constant can be determined using the equation provided [8]:

$$\tau = \frac{L\left(1 + \frac{2\lambda_s}{L}\right)}{2D\kappa\left(\lambda_s\kappa + \tanh\left(\kappa\frac{L}{2}\right)\right)} \tag{23}$$

Taking into consideration that $\lambda_s = 0.46$ nm (Table 1), the best performance for $L < 10^{-4}$ m (Figure 7), it is observed that:
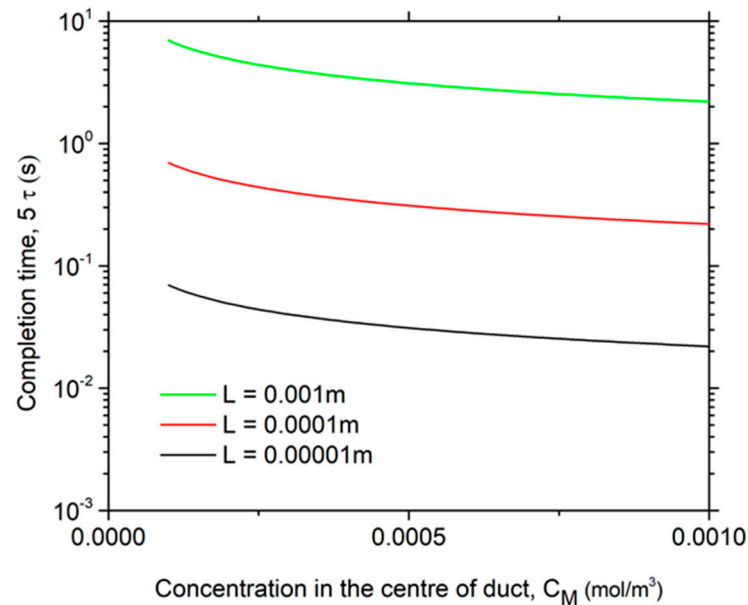
$$\frac{\lambda_s}{L} \approx 4.6 \cdot 10^{-6}$$

and

$$\tanh\left(\kappa\frac{L}{2}\right) \approx 1$$

The time constant equation takes the form:

$$\tau \approx \frac{L}{2D\kappa(\lambda_s\kappa + 1)} \tag{24}$$

Based on Resistor Capacitor (RC) circuit theory, the phenomenon reaches completion in approximately $5\tau$, where $\tau$ represents the time constant. Figure 9 illustrates the completion time as a function of the final concentration in the center of the duct for various duct amplitudes L.



**Figure 9.** Completion time variation $5\tau$ as a function of $C_M$ for different duct widths.

It is noticed that the completion time depends slightly on concentration. Specifically, as the concentration increases, completion time decreases slightly, with the main dependence on the duct width. For duct widths of the order of mm, the completion time is of the order of s, while for duct widths $L \sim 10^{-4}$ m, it is of the order of 0.1 s. All the aforementioned statements apply to a linear regime, provided that the potential is $\varphi_l^{\max}(0) = 0.026$ V. For greater potentials, however, we have every reason to believe that the time will be further reduced, making the method even more attractive for application.

## 5. Conclusions

Considering the results of our study on the application of the electric field induced ion drift method for the accumulation of anthocyanins from winery wastewater, the following is concluded.

A reduction by 90% in anthocyanin concentration in the bulk of a solution is predicted as achievable for duct widths below 1 mm, for applied potentials $\varphi(0)$ in the range of 0.2–0.4 V, and for target concentrations equal to:

$$C_M = 1.2 \cdot 10^{-3} \text{ mol/m}^3$$

The electric field induced ion drift method can be proposed as a promising technique for the purification of wastewater solutions as well as for the accumulation of anthocyanins. This method could also be applied to a range of aqueous food by-products for the recovery of bioactive ingredients.

## References

1. Ioannou, L.A.; Puma, G.L.; Fatta-Kassinos, D. Treatment of winery wastewater by physicochemical, biological and advanced processes: A review. *J. Hazard. Mater.* **2015**, *286*, 343–368. [CrossRef]
2. Mosse, K.P.M.; Patti, A.F.; Christen, E.W.; Cavagnaro, T.R. Winery wastewater quality and treatment options in Australia. *Aust. J. Grape Wine Res.* **2011**, *17*, 111–122. [CrossRef]
3. Oliveira, M.; Duarte, E. Integrated approach to winery waste: Waste generation and data consolidation. *Front. Environ. Sci. Eng.* **2016**, *10*, 168–176. [CrossRef]
4. Rodrigues, R.P.; Gando-Ferreira, L.M.; Quina, M. Increasing Value of Winery Residues through Integrated Biorefinery Processes: A Review. *Molecules* **2022**, *27*, 4709. [CrossRef] [PubMed]
5. Chakka, A.K.; Babu, A.S. Bioactive Compounds of Winery by-products: Extraction Techniques and their Potential Health Benefits. *Appl. Food Res.* **2022**, *2*, 100058. [CrossRef]
6. Rupasinghe, H.V.; Arumuggam, N. Chapter 5: Health benefits of anthocyanins. In *Anthocyanins from Natural Sources: Exploiting Targeted Delivery for Improved Health*; Brooks, M.S.-L., Celli, G.B., Eds.; The Royal Society of Chemistry City: London, UK, 2019; pp. 121–158; ISBN 978-1-78801-736-7.
7. Mattioli, R.; Francioso, A.; Mosca, L.; Silva, P. Anthocyanins: A Comprehensive Review of Their Chemical Properties and Health Effects on Cardiovascular and Neurodegenerative Diseases. *Molecules* **2020**, *25*, 3809. [CrossRef] [PubMed]
8. Nunes, A.N.; Borges, A.; Matias, A.A.; Bronze, M.R.; Oliveira, J. Review Alternative Extraction and Downstream Purification Processes for Anthocyanins. *Molecules* **2022**, *27*, 368. [CrossRef]
9. Lianza, M.; Marincich, L.; Antognoni, F. Review: The Greening of Anthocyanins: Eco-Friendly Techniques for Their Recovery from Agri-Food By-Products. *Antioxidants* **2022**, *11*, 2169. [CrossRef]
10. Bartzis, V.; Sarris, I.E. Time evolution study of the electric field distribution and charge density due to ion movement in salty water. *Water* **2021**, *13*, 2185. [CrossRef]
11. Bartzis, V.; Sarris, I.E. A theoretical model for salt ion drift due to electric field suitable to seawater desalination. *Desalination* **2020**, *473*, 114163. [CrossRef]
12. Bartzis, V.; Sarris, I.E. Electric field distribution and diffuse layer thickness study due to salt ion movement in water desalination. *Desalination* **2020**, *490*, 114549. [CrossRef]
13. Bartzis, V.; Ninos, G.; Sarris, I. Water Purification from Heavy Metals Due to Electric Field Ion Drift. *Water* **2022**, *14*, 2372. [CrossRef]
14. Bartzis, V.; Batrinou, A.; Sarris, I.; Konteles, S.; Strati, I.F.; Houhoula, D. Electric Field Induced Drift of Bacterial Protein Toxins of Foodborne Pathogens *Staphylococcus aureus* and *Escherichia coli* from Water. *Appl. Sci.* **2022**, *12*, 12739. [CrossRef]
15. Sofos, F.; Karakasidis, T.E.; Spetsiotis, D. Molecular dynamics simulations of ion separation in nano-channel water flows using an electric field. *Mol. Simul.* **2019**, *45*, 1395–1402. [CrossRef]
16. Sofos, F.; Karakasidis, T.E.; Sarris, I.E. Effects of channel size, wall wettability, and electric field strength on ion removal from water in nanochannels. *Sci. Rep.* **2022**, *12*, 641. [CrossRef]
17. Sofos, F.A. A water/ion separation device: Theoretical and numerical investigation. *Appl. Sci.* **2021**, *11*, 8548. [CrossRef]
18. Cassone, G. Nuclear Quantum Effects Largely Influence Molecular Dissociation and Proton Transfer in Liquid Water under an Electric Field. *J. Phys. Chem. Lett.* **2020**, *11*, 8983–8988. [CrossRef]
19. Cassone, G.; Sponer, J.; Saija, F. Ab Initio Molecular Dynamics Studies of the Electric-Field-Induced Catalytic Effects on Liquids. *Top. Catal.* **2022**, *65*, 40–58. [CrossRef]
20. Walid Rezanoor, M.; Dutta, P. Combined AC electroosmosis and dielectrophoresis for controlled rotation of microparticles. *Biomicrofluidics* **2016**, *10*, 024101. [CrossRef]
21. Bonnefont, A.; Argoul, F.; Bazant, M. Analysis of diffuse layer on time-dependent interfacial kinetics. *J. Electroanal. Chem.* **2001**, *500*, 52–61. [CrossRef]

22. Bazant, M.Z.; Thornton, K.; Ajdari, A. Diffuse-charge dynamics in electrochemical systems. *Phys. Rev. E* **2004**, *70*, 021506. [CrossRef] [PubMed]

23. Atkins, P.; Atkins, P.W.; de Paula, J. *Atkins' Physical Chemistry*, 10th ed.; Oxford University Press: Oxford, UK, 2014.

24. Monk, P.M.; Mortimer, R.J.; Rosseinsky, D.R. *Electrochromism: Fundamentals and Applications*; John Wiley & Sons: Hoboken, NJ, USA, 2008.

25. Brett, C.M.A. *Electrochemistry: Principles, Methods, and Applications*; Oxford University Press: Oxford, UK, 1994.

26. Debye, P.; Hückel, E. The theory of electrolytes. I. Lowering of freezing point and related phenomena. *Phys. Zeitschrift* **1923**, *24*, 185–206.

27. Kilic, M.S.; Bazant, M.Z.; Ajdari, A. Steric effects in the dynamics of electrolytes at large applied voltages. I. Double-layer charging. *Phys. Rev. E* **2007**, *75*, 021502. [CrossRef] [PubMed]

28. Fedorov, M.; Kornyshev, A. Ionic Liquids at Electrified Interfaces. *Chem. Rev.* **2014**, *114*, 2978–3036. [CrossRef] [PubMed]